

Anomalous resistivity upturn in epitaxial $L2_1$ - Co_2MnAl films

L. J. Zhu^{1,2}, J. H. Zhao²

¹Cornell University, Ithaca, NY 14850, USA

²State Key Laboratory of Superlattices and Microstructures, Institute of Semiconductors, Chinese Academy of Sciences, P. O. Box 912, Beijing 100083, China

We report the controllable growth and the intriguing transport behavior of high-spin-polarization epitaxial $L2_1$ - Co_2MnAl films, which exhibit a low-temperature (T) resistivity upturn with pronounced $T^{1/2}$ dependence, close relevance to structural disorder, and robust independence of magnetic fields. The resistivity upturn turns out to be qualitatively contradictory to weak localization, particle-particle channel electron-electron interaction (EEI), and orbital two-channel Kondo effect, leaving a three-dimensional particle-hole channel EEI the most likely physical source. Our result highlights a considerable tunability of the structural and electronic disorder of magnetic films by varying growth temperature, affording unprecedented insights into the spin polarization and the resistivity upturn.

The full Heusler alloy $L2_1$ - Co_2MnAl has attracted considerable attention in the emerging field of spintronics due to the vanishingly small density of states in minority spin band at Fermi level.^{1,2} Firstly, Heusler ferromagnets with high spin polarization (P) have promise for amazingly high giant magnetoresistance (GMR) in current-perpendicular-plane (CPP) spin valves (SVs) and tunneling magnetoresistance in magnetic tunneling junctions (MTJs).³ Furthermore, the gap or pseudo-gap in the minority spin band significantly suppresses the spin-flip scattering and leads to a very small Gilbert damping constant^{4,5} which is a predominant advantage for low-critical-current spin-torque magnetic memories⁶ as well as long-distance spin wave transport.⁷ Moreover, as proposed by J. Park *et al.*,⁸ high- P Heusler alloys could be an excellent approach to solve the over-rotation problem and to realize ultrafast (~ 100 ps) deterministic switching of the orthogonal spin torque (OST) CPP SVs. The $L2_1$ - Co_2MnAl films are also of great interest in high-sensitivity Hall sensor application due to the giant intrinsic anomalous Hall conductivity arising from Berry phase curvature.^{1,2}

Despite the fascinating properties expected in the fully ordered $L2_1$ - Co_2MnAl , the control of the structural disorder is a crucial issue for the practical Co_2MnAl films in order to obtain a high P . As shown in Fig. 1(a), $L2_1$ - Co_2MnAl crystallizes in the cubic space group $Fm\bar{3}m$ with Co, Mn and Al atoms occupying the Wyckoff positions (1/4, 1/4, 1/4), (0, 0, 0), and (1/2, 1/2, 1/2), respectively. $L2_1$ - Co_2MnAl is predicted to have a P of 75% and a magnetization (M_s) of $\sim 4.04 \mu_B/\text{f.u.}$ (i.e. $\sim 786 \text{ emu}/\text{cm}^3$).^{1,2} $L2_1$ - Co_2MnAl bulk was obtained by induction melting and 10 day annealing at 600-1190°C under a magnetic field of 5 kOe.⁹ However, a $L2_1$ -ordered Co_2MnAl thin film which is of interest for spintronics has barely been achieved despite the extensive efforts.^{3-5,10,11} The Co_2MnAl films usually show a $A2$ or $B2$ ordering when grown on semiconductors^{3-5,10} or when sputtered on MgO (001) with/without a Cr buffer even after post-annealing at up to 500°C.¹¹ Despite the $B2$ phase with Mn-Al swaps preserve the high P and M_s ,^{1,12} the $A2$ phase with Co-Mn swaps significantly reduces both P and M_s as a consequence of the antiparallel alignment of spin moments of Co-Mn or Mn-Mn atoms as revealed by first-principles calculations¹³ and x-ray magnetic circular dichroism measurements.¹⁰ On the other hand, the resistivity (ρ_{xx}) of $L2_1$ - Co_2MnAl films, in addition to P , is critical for achieving a high GMR in CPP SVs. In CPP SVs, not only the interfacial electron scattering but also the bulk region of ferromagnetic layers contribute to the GMR. According to Valet-Fert equation,¹⁴ the GMR is a function of ρ_{xx} and interface and bulk spin-

asymmetry coefficients. The OST CPP SVs with a high- P free layer of $L2_1$ - Co_2MnAl are of great technological interest as sub-ns cryogenic cache memories that can be integrated with Josephson junction logics with 40-100 GHz clock frequency.⁸ Therefore, it is of extreme importance to control the low- T transport behaviors for a better SV performance, for instance, via taking advantage of the structural disorder effects of Co_2MnAl films. Structural disorder such as impurities, strain, and dislocations in Mn-based alloys has been proved to account for the large variations in magneto-optical Kerr effects,^{15,16} Gilbert damping,¹⁷ magnetic anisotropy,¹⁸ anomalous Hall effect,¹⁹ and for the occurrence of electronic disorder physics (e.g. weak localization²⁰ and atomic tunneling effects²¹⁻²³). However, so far, the disorder effects on the transport properties of Co_2MnAl films have been barely investigated.

In this letter, we report an engineering of the structural and electronic disorder in epitaxial $L2_1$ - Co_2MnAl films with high P via controlling the growth temperatures. We observed a low- T resistivity upturn with a $T^{1/2}$ scaling that exhibits close relevance to structural disorder and a robust independence of strong external magnetic fields (H). Such an anomalous resistivity upturn is clarified to arise from three-dimensional (3D) electron-electron interaction (EEI) in a particle-hole diffusion channel.

A series of 40 nm Co_2MnAl films were grown at a rate of ~ 1 nm/min on 150 nm GaAs-buffered semi-insulating GaAs (001) by molecular beam epitaxy (see Fig. 1(b)). In order to tune the structural and electronic disorders of these Co_2MnAl films, the substrate temperature (T_s) was varied to be 50, 150, 250, and 350 °C, respectively. The atomic composition was nominally designed as Co: Mn: Al = 2:1:1, by controlling their fluxes from three thermal-diffusion cells. Each film was capped with a ~ 4 nm MgO protective layer at room temperature. The film thickness was confirmed by the oscillating x-ray reflectivity (XRR) curves at low incidence angles ($2\theta \leq 4^\circ$) in Fig. 1(c). Notably, the oscillation magnitude varies significantly among different samples, indicating that the film homogeneity changes from pretty good at 50 °C to relatively poor at 150 °C, and then gradually improves with T_s further increases to 350 °C. From the x-ray diffraction (XRD) θ - 2θ pattern at high angles ($20^\circ \leq 2\theta \leq 70^\circ$), we can observe the (002) and (004) peaks of Co_2MnAl , indicating an epitaxial growth, a perpendicular c axis, and a $L2_1$ -ordering. A small peak corresponding to the MgO (002) diffraction appears at $2\theta = 42.9^\circ$ for each film, suggesting the epitaxial growth of the capping layer on Co_2MnAl surface. For the sample with $T_s=350$ °C, a new peak unrelated to the $L2_1$ ordering appears at $2\theta = 33.55^\circ$. As

shown in Fig. 1(d), a strong fourfold (111) superlattice peak, the structural fingerprint of $L2_1$ -ordering, was found for each Co_2MnAl film in the XRD φ scans. Such excellent epitaxial compatibility with GaAs is fascinating in efficient pure spin injection into III-V semiconductors via spin pumping that is free of impedance problem and in the development of room temperature ferromagnetic semiconductors via magnetic proximity effect.²⁴ The magnetic properties were measured by a superconducting quantum interference device magnetometer at room temperature. These films were patterned into 60 μm wide Hall bars with adjacent electrode distance of 200 μm using photolithography and ion-beam etching for transport measurements (see Fig. 2(a)). ρ_{xx} was measured in a physical properties measurement system at different T with a 10 μA direct current flowing along Co_2MnAl [110].

High P is a key characteristic of interest for $L2_1$ - Co_2MnAl films. Spin-polarized surface analysis techniques and MTJs with an Al_2O_3 barrier may be useful in determining the surface/interface spin polarization instead of the bulk one of a thick film. The bulk P plays a crucial role in determining the GMR in CPP-SVs. In half metal, a negative anisotropic magnetoresistance (AMR) is argued to reflect a high bulk P .²⁵ The AMR effect basically originates from s - d scattering with conduction electrons scattered from s states to localized d states hybridized by spin-orbit interaction with opposite spin states. In half metal where one of the spin channels is missing at the Fermi level, the s - d scattering only occurs in the existing spin channel, which favors a negative AMR,²⁵ i.e. ρ_{xx} is larger when the current flows orthogonally to magnetization than when parallel. In order to shed light on the P of the $L2_1$ - Co_2MnAl films, we show their magnetoresistance (MR) curves at 300 K in Fig. 2(b). For each film a small MR shows a dip at zero field and gradually increases to peak values at $\sim \pm 15$ kOe, which should be attributed to the AMR effect. As indicated by the magnetization hysteresis in Fig. 2(c), these films show an easy axis along [110] direction and a hard axis along [001] direction. With H gradually increasing from zero to beyond ± 15 kOe,²⁶ the magnetization would gradually rotate from parallel (i.e. [110]) to orthogonal direction (i.e. [001]) with respect to charge current, leading to a variation in measured ρ_{xx} due to the AMR effect. Therefore, the small ρ_{xx} at zero field compared with that at $\sim \pm 15$ kOe can be attributed to the high bulk P of the high-quality $L2_1$ - Co_2MnAl epitaxial films. Intriguingly, we also observed a small MR in the Co_2MnAl films at high H , which scales linearly with H in a broad T range from 2 to 300 K.²⁶ Though not yet fully understood, this high- H MR should be irrelevant to AMR as it does not saturate even at 8 T but the magnetic moment aligns completely along film normal when H is beyond ± 15 kOe. Spin wave scattering can be excluded as thermal magnons are unlikely to be excited at T as low as 2 K. In addition, we may also use M_s as an index of the bulk P of the $L2_1$ - Co_2MnAl films. There is a wide consensus that a high M_s in a Co_2MnAl sample is always accompanied by a high bulk P .^{1,3,12,13} As mentioned above, $L2_1$ - Co_2MnAl is expected to have a high P and M_s that are robust against Mn-Al swaps; the occurrence of Co-Mn swaps would significantly reduce the P and M_s at the same time. As shown in Fig. 2(d), all the films with T_s beyond 150 $^\circ\text{C}$ shows high M_s , ranging from 764-912 emu/cm^3 , suggesting their few Co-Mn swaps and high P . The slightly higher M_s than theoretical value may be probably due to a Co-rich¹³

or Mn-rich composition of these films.¹² Here, Co-Al swaps which were predicted to enhance M_s by increasing the magnetic moment of each Co atom¹³ can be ruled out by the strong (002) and (111) XRD peaks. The relatively small M_s of 338 emu/cm^3 at $T_s = 50$ $^\circ\text{C}$ indicates an increased Mn-Mn antiferromagnetic coupling^{10,13} as the strong (001) and (111) XRD peaks make enhanced Co-Mn swaps unlikely. Taking into account the evident presence of $L2_1$ -ordering in XRD patterns, the negative AMR, and the large M_s , the high P may be established in these films.

Now we turn to the T -dependent electrical transport behaviors of these films. Figure 3(a) shows the zero-field ρ_{xx} of the Co_2MnAl films as a function of T . Each film shows a resistivity minimum (ρ_{xx0}), beyond which ρ_{xx} increases monotonically with T mainly due to the increasing phonon scattering. The apparent nonlinearity of ρ_{xx} - T curve at high T should be attributed to a weak magnon scattering, which further indicates that $L2_1$ - Co_2MnAl is not a complete half metal. In the following, we show that the low- T resistivity upturns in these Co_2MnAl films most likely arise from disorder-enhanced EEI in a particle-hole channel. The 3D particle-hole channel EEI is expected to give a $T^{1/2}$ -dependent correction to ρ_{xx} as a consequence of the correlation between wave function of the added electron and the wave functions of the occupied electrons that are nearby in energy.²⁷ In the presence of a nonzero H , the correction includes a $S_z=0$ Hartree contribution and a $S_z=\pm 1$ triplet contribution. The former involves electrons with the same spin, and is unaffected by the splitting of spin up and down bands; while the latter should be independent of H in a ferromagnetic system because both Zeeman splitting (~ 0.68 meV at 6 T) and the temperature (4.3 meV at 50 K) are negligible compared with the ferromagnetic exchange splitting (~ 10 eV). Therefore, 3D particle-hole channel EEI in a ferromagnet can be signified by a $T^{1/2}$ -dependent resistivity upturn with an H independence and a close correlation to disorder.

Figures 3(b) plots the resistivity variation at $H = 0$ T as a function of T for the Co_2MnAl films with different T_s . The resistivity increase, $\Delta\rho_{xx}$ ($\Delta\rho_{xx} = \rho_{xx} - \rho_1$, with the offset ρ_1 determined from the best linear fit of $\rho_{xx}T^{1/2}$), varies linearly with $T^{1/2}$ when T drops below a typical temperature T_0 . T_0 (ρ_1) was estimated to be ~ 15.2 (128.1), ~ 27.8 (155.0), ~ 30.0 (151.0), ~ 17.9 (156.1) K ($\mu\Omega$ cm) for $T_s = 50, 150, 250,$ and 350 $^\circ\text{C}$, respectively. The slope $k = d\rho_{xx}/d(T^{1/2})$ reflects the strength of the EEI and the diffusion constant of the film, i.e. an increase in k suggests an enhancement of the EEI and/or a reduction of diffusion constant.²⁷ The $T^{1/2}$ dependence of the resistivity upturns in different samples can be visualized more directly by collapsing the T -dependent $\Delta\rho_{xx}$ data of different samples onto single scaling curve of $-\Delta\rho_{xx}/kT_0^{1/2} = (T/T_0)^{1/2}$ for $T/T_0 < 1$. From Fig.3(c) we can see that $\log(-\Delta\rho_{xx}/kT_0^{1/2})$ scales linearly with $\log(T/T_0)$ with a slope of 1/2 when $T/T_0 < 1$ for the Co_2MnAl samples with different T_s . It should be mentioned that the high-field MR which even exists at 300 K (see Fig. 2(b)) is unlikely to be related to the $T^{1/2}$ dependence of $\Delta\rho_{xx}$ due to the EEI. In order to establish more rigorously the particle-hole channel EEI in these Co_2MnAl films, we examined the effect of H on the T dependence of ρ_{xx} . As an example, we show $\Delta\rho_{xx}$ for $T_s = 150$ $^\circ\text{C}$ under various H of 0, 3, and 6 T in Fig. 3(d). The magnetic fields show no measurable effect on the T dependence: ρ_{xx} scales linearly with $T^{1/2}$ at below T_0 ($T_0 \sim 27.8$ K) and T_0 and k are apparently independent of H , strongly suggesting a spin-

independent origin of the resistivity upturns. The same features hold for other films with different T_s . As plotted in Fig. 3(e), k first increases from the minimum of $0.142 \mu\Omega \text{ cm/K}^{1/2}$ at 50°C to the maximum of $0.182 \mu\Omega \text{ cm/K}^{1/2}$ at 150°C , and finally goes down to $0.169 \mu\Omega \text{ cm/K}^{1/2}$ at 350°C , which reflects the evolution of the EEI strength and the electron diffusion constant with structural disorder.²⁷ The T_s dependence of k in the Co_2MnAl films excellently agrees with those of M_s and film homogeneity indicated by the XRR oscillation amplitude.

We now discuss the evolution of the structural disorder with T_s in these high P films and their close relevance to the resistivity upturn. Figure 4(a) summarizes as a function of T_s the lattice constant c of the Co_2MnAl films determined from the Co_2MnAl (004) XRD peaks. As schematically shown, their much larger c than the bulk value of 5.755 \AA indicate a strong strain in these films probably due to the large lattice mismatch with GaAs ($a_{\text{GaAs}}=5.662 \text{ \AA}$), which also makes these films likely to have high-density dislocations. c firstly drops from 5.880 \AA at 50°C to 5.810 \AA at 150°C , and then monotonically goes up to 5.850 \AA at 350°C , suggesting a significant variation in the strain strength. Compared to other samples, the slightly short c axis at 150°C likely indicates a relatively high degree of strain relaxation and a high density of the dislocations. The evolution of the film disorder with T_s can be further proved by the intensity of XRD peaks. Figure 4(b) shows the integrated intensity of Co_2MnAl (004) peaks (I_{004}) normalized by the real-time monitored and recorded intensity of the incidence x-ray beam during the measurements. I_{004} first drops remarkably by a factor of 10 as T_s increases from 50 to 150°C , and then gradually increases as T_s further increases towards 350°C , the tendency of which excellently coincides with those of homogeneity and strain. Intriguingly, in $L1_0$ -MnGa and $L1_0$ -MnAl films,^{19,21,22} if we use ρ_{xx0} (approximately the residual resistivity due to static impurity scattering) and the thermal contribution to the resistivity ($\rho_{\text{them}}=\rho_{xx}-\rho_{xx0}$) to quantify the strengths of structural disorder and the phonon and magnon scattering, respectively, the phonon and magnon scattering can be found to become increasingly suppressed with enhancing structural disorder. Therefore, ρ_{them} also reflects the degree of structural perfection. The same is also true for these Co_2MnAl films as ρ_{them} in Fig. 4(c) varies with T_s in an analogue manner of strain and I_{004} . We also plotted ρ_{xx0} as a function of T_s in Fig. 4(d), which leads to the virtually same conclusion on how the structural disorder varies with T_s except that the slight recovery of ρ_{xx0} at $T_s=350^\circ\text{C}$ in comparison to $T_s=250^\circ\text{C}$ may be related to the appearance of the peak at $2\theta = 33.55^\circ$ and seems to be less important to the EEI. In a word, the $T^{1/2}$ scaling, the H -independence, and the disorder nature of low- T resistivity upturns are highly consistent with a particle-hole channel EEI mechanism.

We further clarify that particle-hole channel EEI is the most likely physical source of the low- T resistivity upturns. Besides the particle-hole channel EEI, there are at least three alternative effects that can give rise to a $T^{1/2}$ -dependent resistivity upturn: (i) 3D weak localization, (ii) 3D EEI in a particle-particle channel, and (iii) orbital two-channel Kondo (2CK) effect due to resonant two-level system (TLS) scattering. An explanation of quantum correction due to 3D weak localization can be safely excluded here as the strong external magnetic field H and the giant internal magnetic field due to ferromagnetic

exchange splitting of $\sim 10^5 \text{ T}$ can completely destroy the quantum interference phase of the electron wave function on the time-reversed path and thus forbid the weak localization.²⁷ The 3D EEI in a particle-particle channel is expected to give a $T^{1/2}$ -dependent correction to the resistivity at very weak magnetic field, however, a strong magnetic field can also easily destroy it. A $T^{1/2}$ -dependent resistivity upturn is also expected in an orbital 2CK effect which occurs when a pseudospin-1/2 of structural TLS (where an atom or atom group with small effective mass coherently tunnels between two nearby positions) equally couples to two spin channels of conduction electrons via resonant scattering.²⁸ The orbital 2CK effect is manifested in electrical transport by a unique low- T resistivity upturn which scales with $\ln T$, $T^{1/2}$ and T^2 in three distinct T regimes, respectively.^{21,23} Importantly, an external magnetic field should have no sizeable influence on the resistivity upturn because the electron spin variables are irrelevant to the Kondo coupling between the TLS and conduction electrons, and Zeeman splitting is negligible in comparison to the Fermi energy. The orbital 2CK fixed point and the resultant $T^{1/2}$ dependence also appear to be robust against a weak population asymmetry of the two spin channels.²¹⁻²³ However, the P appears to be high in these $L2_1$ - Co_2MnAl films as discussed above. The strong channel asymmetry due to the high P would lead to different tunneling rates of a TLS for two spin channels and decouple the TLSs from one spin channel, and consequently destroy the 2CK physics and the $T^{1/2}$ dependence of resistivity. Therefore, the 2CK effect seems unlikely here despite the agreements in the disorder dependence, the $T^{1/2}$ scaling, and the H -independence of resistivity upturn. On the other hand, in contrast to the $L1_0$ -MnGa and $L1_0$ -MnAl films displaying the orbital 2CK effect,^{21,23} these $L2_1$ - Co_2MnAl films show a clear absence of a $\ln T$ dependence in the resistivity at higher energy scale, which further implies the inapplicability of 2CK explanation here. Here, we mention that our systematic study on Co_2MnAl films with controlled disorder may also suggest a diffusion channel EEI mechanism for the low- T resistivity upturns in Heusler $\text{Co}_2\text{Mn}_{0.25}\text{Ti}_{0.75}\text{Al}$,²⁰ Co_2MnSi ,²⁹ and Co_2MnGa films,³⁰ while the weak localization explanation in the literature seems problematic.

In conclusion, we have for the first time presented the controllable epitaxial growth and the transport behavior of $L2_1$ - Co_2MnAl films with strong P . The $T^{1/2}$ dependence, the H independence, and the disorder relevance of the low- T resistivity upturn are well consistent with the 3D particle-hole channel EEI, while the weak localization, the particle-particle channel EEI and the orbital 2CK physics are conclusively excluded. The unprecedented tunability of the structural and electronic disorders leads to the insight into the P and the origin of the resistivity upturn. The controllable epitaxial growth of highly ordered $L2_1$ - Co_2MnAl films shows promise for spin pumping spin injection into III-V semiconductors and for developing room temperature ferromagnetic semiconductors utilizing magnetic proximate effect. These results would be also helpful in better understanding of the transport properties of various Heusler films and in their spintronic applications such as ultrafast reliable cryogenic OST CPP-SV memories.

This work was partly supported by MOST of China (Grant No. 2015CB921503), NSFC (Grant No. 61334006), and NSF MRSEC program (Grant No. DMR-1120296).

- ¹J. Kibler and C. Felser, *Phys. Rev. B* **85**, 012405 (2012).
- ²J.-C. Tung and G.-Y. Guo, *New J. Phys.* **15**, 033014 (2013).
- ³M. Oogane, Y. Sakuraba, J. Nakata, H. Kubota, Y. Ando, A. Sakuma, and T. Miyazaki, *J. Phys. D: Appl. Phys.* **39**, 834-841 (2006).
- ⁴S. Qiao, S. Nie, J. Zhao, Y. Huo, Y. Wu, and X. Zhang, *Appl. Phys. Lett.*, **103**, 152402 (2013).
- ⁵W. Yan, H. Wang, W. Du, J. Zhao, and X. Zhang, *J. Phys. D: Appl. Phys.* **49**, 065005 (2016).
- ⁶L. Liu, C.-F. Pai, Y. Li, H. W. Tseng, D. C. Ralph, and R. A. Buhrman, *Science* **336**, 555-558 (2012).
- ⁷Y. Kajiwara, K. Harii, S. Takahashi, J. Ohe, K. Uchida, M. Mizuguchi, H. Umezawa, H. Kawai, K. Ando, K. Takanashi, S. Maekawa, and E. Saitoh, *Nature* **464**, 262 (2010).
- ⁸J. Park, D. C. Ralph, and R. A. Buhrman, *Appl. Phys. Lett.* **103**, 252406 (2013).
- ⁹R. Y. Umetsu, K. Kobayashi, A. Fujita, R. Kainuma, and K. Ishida, *J. Appl. Phys.* **103**, 07D718 (2008).
- ¹⁰K. K. Meng, S. L. Wang, P. F. Xu, L. Chen, W. S. Yan and J. H. Zhao, *Appl. Phys. Lett.* **97**, 232506 (2010).
- ¹¹Y. Sakuraba, J. Nakata, M. Oogane, H. Kubota, Y. Ando, A. Sakuma, T. Miyazaki, *Jpn. J. Appl. Phys.* **44**, 6535-6537 (2005).
- ¹²K. Özdoğan, E. Şaşıoğlu, B. Aktaş, and I. Galanakis, *Phys. Rev. B* **74**, 172412 (2006).
- ¹³J. Kudrnovsky, V. Drchal, and I. Turek, *Phys. Rev. B* **88**, 014422 (2013).
- ¹⁴T. Valet and A. Fert, *Phys. Rev. B* **48**, 7099 (1993).
- ¹⁵L. J. Zhu, L. Brandt, J. H. Zhao, and G. Woltersdorf, *J. Phys. D: Appl. Phys.* **49**, 245001 (2016).
- ¹⁶L. Zhu, L. Brandt, and J. Zhao, *J. Phys. D: Appl. Phys.* **49**, 415001 (2016).
- ¹⁷M. Oogane, T. Kubota, H. Naganuma, and Y. Ando, *J. Phys. D: Appl. Phys.* **48**, 164012 (2015).
- ¹⁸L. Zhu, S. Nie, K. Meng, D. Pan, J. Zhao and H. Zheng, *Adv. Mater.* **24**, 4547 (2012).
- ¹⁹L. J. Zhu, D. Pan, and J. H. Zhao, *Phys. Rev. B* **89**, 220406 (R) (2014).
- ²⁰M. Aftab, G. H. Jaffari, S. K. Hasanain, T. A. Abbas and S. I. Shah, *J. Phys. D: Appl. Phys.* **47**, 475001(2012).
- ²¹L. J. Zhu, S. H. Nie, P. Xiong, P. Schlottman, and J. H. Zhao, *Nat. Commun.* **7**, 10817 (2016).
- ²²L. J. Zhu, S. H. Nie, J. H. Zhao, *Phys. Rev. B* **93**, 195112 (2016).
- ²³L. Zhu, G. Woltersdorf, J. Zhao, *Sci. Rep.* **6**, 34549 (2016).
- ²⁴S. H. Nie, Y. Y. Chin, W. Q. Liu, J. C. Tung, J. Lu, H. J. Lin, G. Y. Guo, K. K. Meng, L. Chen, L. J. Zhu, D. Pan, C. T. Chen, Y. B. Xu, W. S. Yan, and J. H. Zhao, *Phys. Rev. Lett.* **111**, 027203 (2013).
- ²⁵S. Kokado, M. Tsunoda, K. Harigaya, and A. Sakuma, *J. Phys. Soc. Jpn.* **81**, 024705 (2012).
- ²⁶See supplementary materials at xxx for further information on MR behaviors at 2 K and out-of-plane magnetization hysteresis for L_{21} - Co_2MnAl films with different T_s .
- ²⁷P. A. Lee and T. V. Ramakrishnan, *Rev. Mod. Phys.* **57**, 287-337 (1985).
- ²⁸G. Zaránd, *Phys. Rev. B* **72**, 245103 (2005).
- ²⁹L. J. Singh, Z. H. Barber, Y. Miyoshi, W. R. Branford, and L. F. Cohen, *J. Appl. Phys.* **95**, 7231 (2004).
- ³⁰C. D. Damsgaard, M. C. Hickey, S. N. Holmes, R. Feidenhans'l, S. O. Mariager, C. S. Jacobsen, and J. B. Hansen, *J. Appl. Phys.* **105**, 124502 (2009).

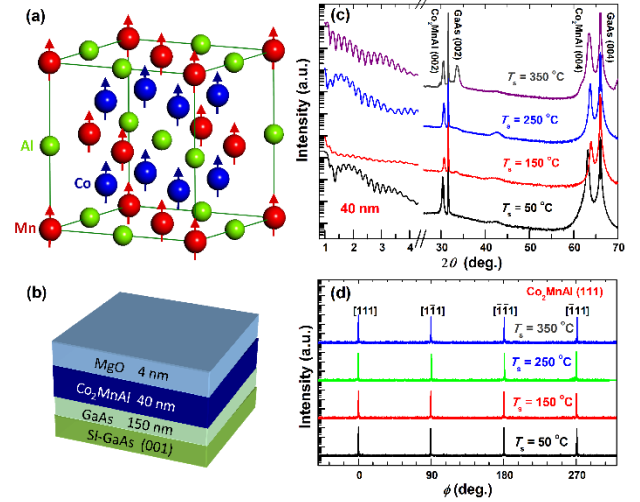


FIG. 1 Schematic of (a) L_{21} - Co_2MnAl lattice structure and (b) Sample structure; (c) XRR and XRD patterns and (d) ϕ scans along (111) for Co_2MnAl films grown at different T_s .

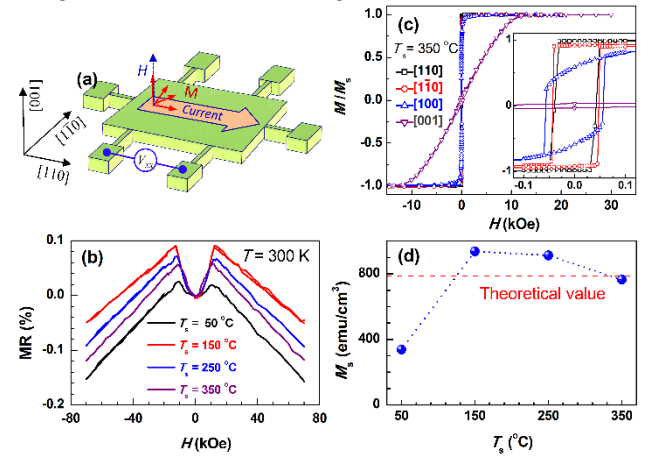


FIG. 2 (a) Hall bar geometry with respect to the crystalline directions of Co_2MnAl ; (b) MR at 300 K; (c) Normalized magnetization hysteresis at 300 K ($T_s = 350^\circ\text{C}$) along [110], $[1\bar{1}0]$, [100] and [001] directions, respectively, the inset is close-up view at small fields; and (d) M_s for the L_{21} - Co_2MnAl film with different T_s . The red dashed line in (d) refers to the theoretical value of M_s .

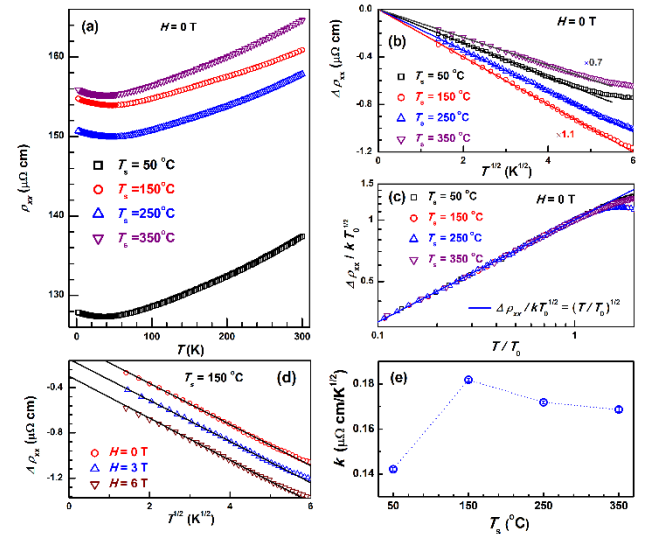


FIG. 3 (a) T vs ρ_{xx} , (b) $\Delta\rho_{xx}$ vs $T^{1/2}$ ($H = 0$ T), (c) log-log plot of $-\Delta\rho_{xx}/kT_0^{1/2}$ vs T/T_0 ($H = 0$ T), (d) $\Delta\rho_{xx}$ vs $T^{1/2}$ ($H = 0, 3,$ and 6 T), and (e) k for Co_2MnAl films with different T_s . For clarity, $\Delta\rho_{xx}$ in (b) is multiplied by a factor of 0.7 and 1.1 for $T_s = 50$ and 150°C , respectively; the curves at 3 and 6 T in (d) were artificially shifted by -0.16 and $-0.32 \mu\Omega\text{ cm}$, respectively.

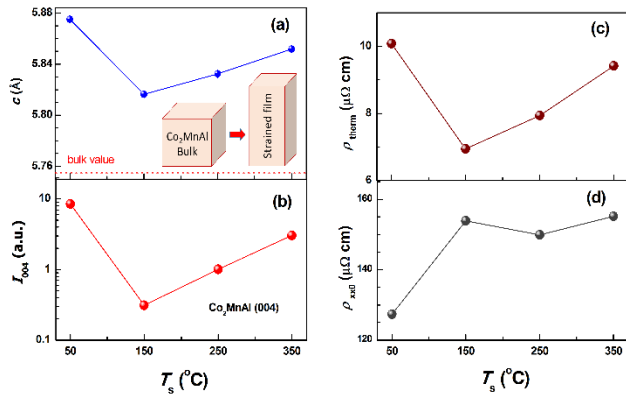


FIG. 4 (a) c , (b) I_{004} , (c) ρ_{therm} , and (d) ρ_{xx0} for Co_2MnAl films with different T_s . The inset in (a) shows schematically a strained Co_2MnAl lattice cell and a bulk one; the red dashed line shows the bulk value of c .